

## Full-scale tests and finite element analysis of arched corrugated steel roof under static loads

X. P. Wang, C. R. Jiang, G. Q. Li and S. Y. Wang

*School of Civil Engineering and Architecture, Wuhan University of Technology, Wuhan, 430070, China*

*(Received November 19, 2005, Accepted June 22, 2007)*

**Abstract.** Arched Corrugated Steel Roof (ACSR) is a kind of thin-walled steel shell, composing of arched panels with transverse small corrugations. Four full-scale W666 ACSR samples with 18m and 30m span were tested under full and half span static vertical uniform loads. Displacement, bearing capacities and failure modes of the four samples were measured. The web and bottom flange in ACSR with transverse small corrugations are simplified to anisotropic curved plates, and the equivalent tensile modulus, shear modulus and Poisson's ratio of 18m span ACSR were measured. Two 18 m-span W666 ACSR samples were analyzed with the Finite Element Analysis program ABAQUS. Base on the tests, the limit bearing capacity of ACSR is low, and for half span loading, it is 74-75% compared with the full span loading. When the testing load approached to the limit value, the bottom flange at the sample's bulge place locally buckled first, and then the whole arched roof collapsed suddenly. If the vertical loads apply along the full span, the deformation shape is symmetric, but the overall failure mode is asymmetric. For half span vertical loading, the deformation shape and the overall failure mode of the structure are asymmetric. The ACSR displacement under the vertical loads is large and the structural stiffness is low. There is a little difference between the FEM analysis results and testing data, showing the simplify method of small corrugations in ACSR and the building techniques of FEM models are rational and useful.

**Keywords:** Arched Corrugated Steel Roof (ACSR); full-scale samples; static tests; transverse small corrugations; anisotropic plates; finite element analysis.

---

### 1. Introduction

Arched Corrugated Steel Roof (ACSR) is a kind of thin-walled doubly corrugated shell. ACSR is composed of T or U-section (Fig. 1) arched panel units, which are connected together between the longitudinal side edges by lockstitching machine. The production procedure of ACSR is consisted of four steps: the 0.6-1.6 mm thick steel sheet is cold-deformed to a straight panel with U or T section (Fig. 2a); the straight panel is roll-formed again to one arched panel unit with transverse small corrugations (Fig. 2b); three to five arched panel units are connected together between the longitudinal side edges on the ground, generating a suspending unit; the suspending units are suspended to the suitable places and connected together, forming the whole arched roof. Fig. 3 is an engineering example in China. ACSR first appeared in North America and was used in the construction of metal arch type buildings such as farm buildings and warehouses (Wang 1999, Zhang 2000, Xu 2001).

---

†Correspondence Author, E-mail: whut\_wangxp@yahoo.com.cn

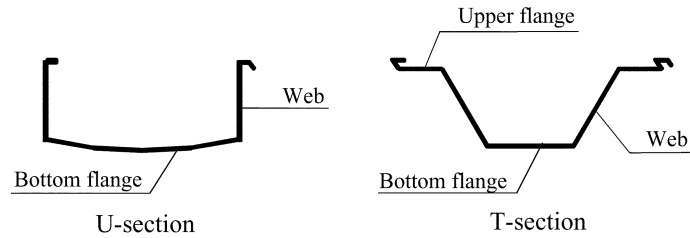


Fig. 1 Two sections of arched panel units

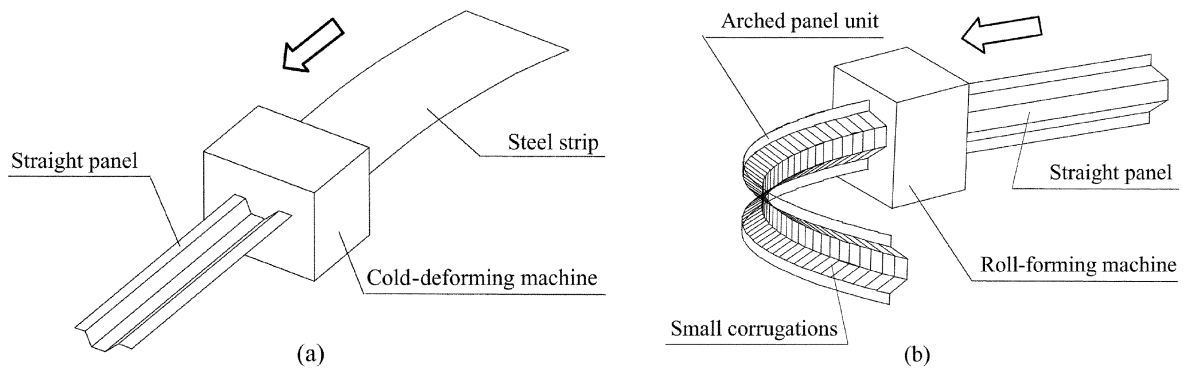


Fig. 2 Production schematic drawing of one arched panel unit



Fig. 3 Engineering example of ACSR

ACSR was imported into China at the end of 1980s. Because of lightweight, low cost, short construction period, fine-looking appearance and good waterproof property, this kind of structure is widely used in the construction of warehouses, workshops, markets and stations. The largest span has reached to 36 m in China, and ACSR roof with the area of 10000 m<sup>2</sup> can be built up within 20 days (Liu 1999, Zhang 2000).

Since there are a large number of irregular transverse corrugations and residual stresses caused by

processing in ACSR, the structural analysis seems to be very complicated. The early related research work mainly concentrated on the simplify analysis method. For the curved panels of corrugated sheets, the effect of small corrugations in corrugated sheets was ignored and the curved panels were treated as anisotropic curved plates (Abdel-Sayed 1970, Marzouk 1975). The doubly corrugated shells (ACSR) were studied with finite element method and the small corrugations were replaced by an equivalent orthographic material of uniform thickness (Herbert 1976). Testing is a way to obtain the equivalent modulus of the corrugated plates (Jorgenson 1982, Hahn 1992, Friedman 1994, Featherston 1998). In Benussi's research work (Benussi 1986), each arched panel unit in ACSR was regarded as an arch beam while the rigidity of the beam was calculated base on the effective width of the webs and flanges. Xu (2001) performed two types of compressive tests; namely, the corner and flange-section test, and full-section test, and the influences of panel curvatures and transverse corrugations on buckling behavior of the corrugated ACSR curved panels were investigated. In addition, a series of full-scale tests of ACSR structures made in different companies were performed, covering different spans, such as 15 m, 18 m, 24 m, 30 m, 33 m (Airumyan 1997, Liu 1999, Wang 1999, Zhang 2000). All the full-scale testing results can be used as the structural application basis and verification of a simplified method. The related design and construction code on ACSR structure had been compiled in China (CECS167 2004).

In this paper, a kind of W666 ACSR, which was developed by Wuhan Iron and Steel (Group) Company, was tested and analyzed. Four full-scale samples were tested, including different spans and loading methods. The web and bottom flange with small transverse corrugations are simplified to anisotropic curved plates, and the equivalent constants were measured. Base on the simplified method, two 18m-span W666 ACSR were analyzed with the finite element analysis program ABAQUS, and the analysis results are compared with the testing data.

## 2. Testing techniques

### 2.1 Samples

Four full-scale W666 ACSR samples with T section were tested. Each sample was composed together with three arched panel units on the longitudinal side edges (See Fig. 4), possessing the total



Fig. 4 Part of an 18 m span sample

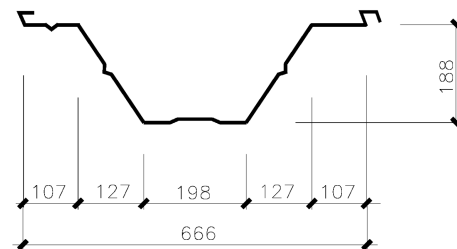


Fig. 5 Section dimensions of W666 panel unit

Table 1 Detail information of four samples

Sample labels	Span (m)	Arch rise (m)	Nominal thickness (mm)	Loading position	Testing day
T18-H	18	4.5	1.0	Half span	1998. 06. 12
T18-F	18	4.5	1.0	Full span	1997. 10. 24
T30-H	30	7.5	1.2	Half span	1998. 09. 13
T30-F	30	7.5	1.2	Full span	1998. 04. 27

width of 2 m. The T section dimensions of each arched panel unit are shown in Fig. 5.

The samples include two spans: 18 m and 30 m. The ratios between arch rise and span are all 0.25, meaning the arch rises of 18 m and 30 m span samples are separately 4.5 m and 7.5 m. The material type of the four samples is China steel Q235, having the nominal yield stress 235 N/mm<sup>2</sup>. The nominal thickness is 1.0 mm for 18 m span samples, and 1.2 mm for 30 m span ones. The 18 m span samples were made of continual hot-dip zinc-coated steel strips, while the 30 m span samples were made of colored paint coat steel strips. All the steel strips were manufactured by Wuhan Iron and Steel (Group) Company with 1000 mm wide.

Detail information of four samples is listed in Table 1.

## 2.2 Support and loading method

Two longitudinal ends of the samples were simply designed to pin support (Fig. 6 and Fig. 7). For one support, there is a steel box filled with concrete, as shown in Fig. 6. The two ends of each sample were separately poured in the concrete of the two steel boxes. At each end, three steel roll tubes with 48 mm diameters were set between the concrete pier and the bottom of the steel box. The steel boxes at two ends were linked with 320 mm steel bars, and three 50 kN load cells were separately set in the middle of the three steel bars in order to measure the horizontal thrust (see Fig. 7).

A series of vertical centralized loads  $P$  were added on the samples instead of the uniform vertical loads. For the full span loading situation, there are respectively 15 and 19 loading points for 18 m and 30 m span samples, which are distributed uniformly along the span, as shown in Figs. 8 and Fig. 9. For the half span loading, the loads were applied on the left half span and the applying points were same as those in Figs. 8 and 9, while the centralized load  $P$  at the middle point was change to  $0.5 P$ .

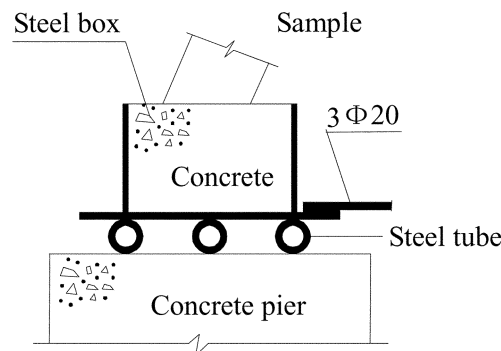


Fig. 6 Longitudinal support detail of samples



Fig. 7 Support photo of 30 m span sample

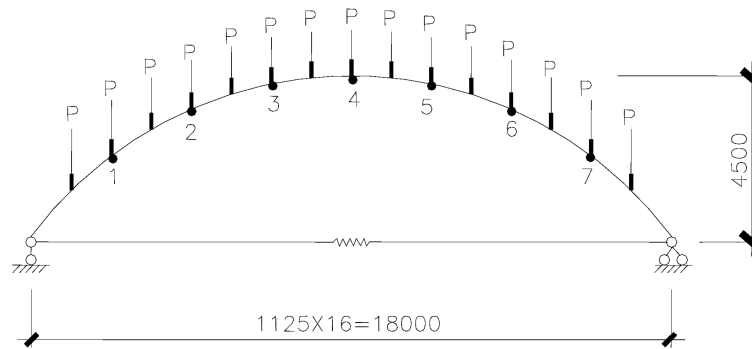


Fig. 8 Loading points of 18 m span samples

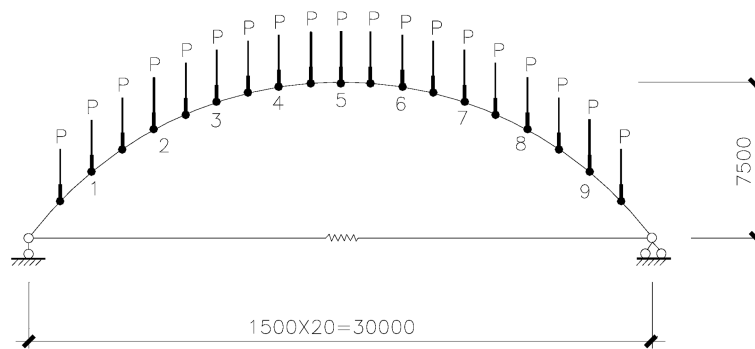


Fig. 9 Loading points of 30 m span samples

Because the outside surface of each ACSR sample is very smooth and slope, the direct applying of the vertical centralized loads is difficult. Some loading measures were adopted on the testing site. Fig. 10 is the photo of the loading method. For each loading point, there are three steel components with 300 mm long and 6 mm thick. Each component has the similar section with the arched panel unit in Fig. 5 and was connected with the panel by six 6 mm diameter bolts. In order to reduce the local



Fig. 10 Loading method and set of 18 m span samples

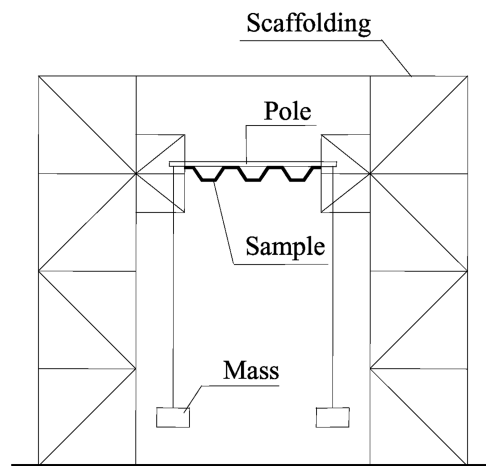


Fig. 11 Schematic drawing of scaffolding

stress concentration, protect the samples and distribute the centralized loads, a piece of rubber with 10 mm thick was put between one component and the sample surface. For each loading point, three components were welded together with a steel angle served as loading pole. Two loading hooks were separately hanged at the two ends of each angle pole through the iron wires. For every loading step, the iron bricks of all loading points should be hanged on the corresponding hooks at the same time (Fig. 7). On the side of each loading hook should stand a person. On the testing site of 30 m span sample T30-F in Table 1, 38 persons took part in the loading process.

In order to prevent the samples from inclining, the scaffolding was built so that each sample could only move vertically and could not buckle out of plane. The schematic drawing and photo of the scaffolding are separately shown in Fig. 11 and Fig. 12.



Fig. 12 Photo of the scaffolding

### 2.3 Displacement measurement method

After each step loading, the structural displacement was measured.

Whether for full or half span loading, there are respectively 7 and 9 displacement measuring points for the 18 m and 30 m span samples, as shown in Fig. 8 and Fig. 9. For each point, the measurement content includes horizontal and vertical displacements.

Measuring of the vertical displacement is simple. For each measurement point of a sample, a leveling rod was hanged on the side edge of the sample. A leveling instrument was used to read the data of the rods before and after each loading step. The vertical displacement for some loading level can be obtained base on the difference between two times reading data.

The horizontal displacement for every loading point on the samples was obtained as following steps:

1. A theodolite was set up at a suitable place in front of the sample (Fig. 13);
2. The horizontal distance  $D_i$  between the theodolite and every measurement point was measured by use of the theodolite;

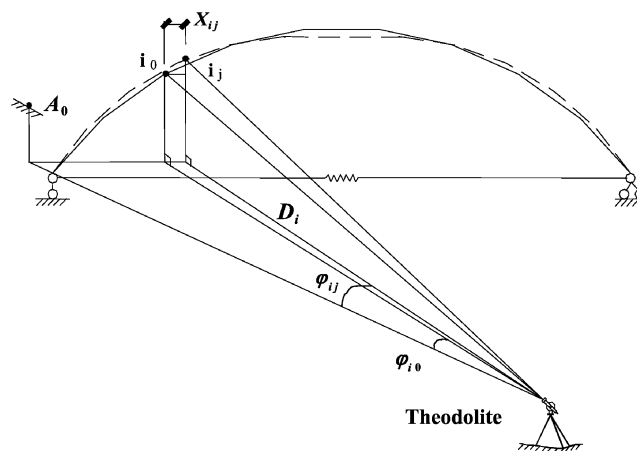


Fig. 13 Measurement principle of horizontal displacement

3. Before loading, the horizontal angle  $\varphi_{i0}$  ( $i = 1, 2, 3, \dots$ ) was read between some fixed point  $A_0$  and each measurement point  $i_0$ ;
4. When the loading got to the  $j$  level, the point  $i$  moved from  $i_0$  to  $i_j$ , the horizontal angle  $\varphi_{ij}$  ( $i = 1, 2, 3, \dots$ ) was also read between point  $A_0$  and  $i_j$ ;
5. From initial situation to the  $j$  loading level, the horizontal displacement  $X_{ij}$  at point  $i$  can be calculated by the following equation:

$$X_{ij} = D_i \cdot \text{tg}(\varphi_{ij} - \varphi_{i0}) \quad (1)$$

where  $i = 1, 2, 3, \dots, j$  is the loading level number.

### 3. Development of finite element model

#### 3.1 Simplify of corrugated webs and flanges

As stated before, the shapes of the irregular transverse small corrugations in the webs and bottom flanges are complicated (see Fig. 4), and the depth and width of each transverse corrugation in the webs are different along the corrugating direction. For the convenience of analysis, the web and bottom flange were separately simplified to anisotropic uniform curved plates and the equivalent thickness was considered as uniform 1.0 mm (see Fig. 14). The equivalent average tensile modulus, shear modulus and Poisson's ratio were measured by tensile and shear tests. The tensile and shear specimens were cut from an 18 m span W666 ACSR panel unit, whose dimensions and material were same as T18-H and T18-F in Table 1.

For the web and bottom flange specimens with irregular transverse corrugations, base on the tensile and shear testing results (Wang 1999), the relationships between the tensile or shear loads and the corresponding deformation are nonlinear after the loads applied, leading to the variation of the equivalent modulus at the different loading level. This phenomenon was caused by the plastic deformation in the corrugated webs and bottom flanges. For the application convenience, the load-deformation curves are replaced by the straight trend lines, which are considered as the calculation basis of equivalent elastic modulus. Table 2 provides the measurement averaged equivalent values of the elastic tensile modulus, shear modulus and Poisson's ratio in two directions, which are the basis of the structural analysis of 18 m span W666 ACSR.

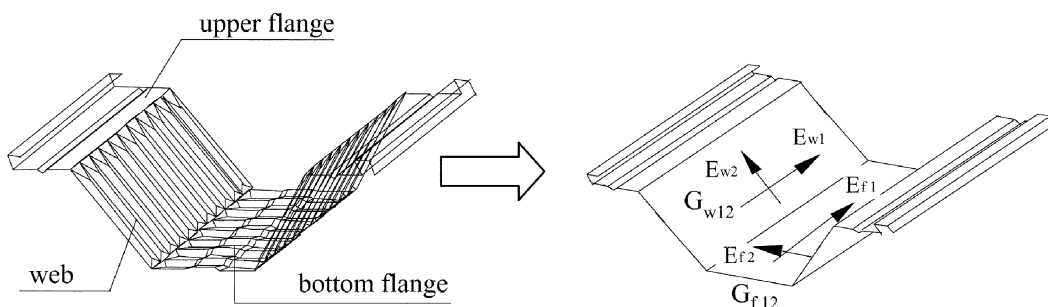


Fig. 14 Simplify method of web and bottom flange

Table 2 Measurement results of equivalent elastic modulus of corrugated plates

Plates types	Material types	Equivalent elastic modulus ( $\times 10^5$ N/mm <sup>2</sup> )			Equivalent Poisson's ratio	
		$E_1$	$E_2$	$G_{12}$	$\mu_{12}$	$\mu_{21}$
Web	anisotropic	0.24	0.48	0.60	0.006	0.045
Bottom flange	anisotropic	0.09	0.74	0.05	0.02	0.07

For an anisotropic plate, it is common knowledge that the following relationship must be satisfied:

$$E_x \mu_y = E_y \mu_x \quad (2)$$

In Eq. (2),  $E_x$  and  $E_y$  are separately the tensile modulus in  $X$  and  $Y$  directions, while  $\mu_x$  and  $\mu_y$  are the Poisson's ratios in two directions.

For the tensile specimens cut from the webs and bottom flanges in 18 m span W666 ACSR, it is obvious that the measurement equivalent elastic tensile modulus and Poisson's ratios in Table 2 do not meet Eq. (2) due to the measurement error of the equivalent Poisson's ratio. Because the equivalent Poisson's ratio is almost 0 for the irregular corrugation plates, it is difficult to obtain an accurate measurement results.

### 3.2 Building of finite element model

In order to prove the validity of the simplify method of corrugated webs and flanges, the 18 m-span W666 ACSR composed of three panel units was analyzed with the finite element non-linear analysis program ABAQUS version 6.4 base on the parameters in Table 2, while the tensile equivalent elastic modulus is assumed to be equal to the compressive one. The structural analysis results, such as the ultimate strength, failure modes and deformation were compared with the full-scale testing data. For the sake of simulating the post buckling response, geometric nonlinear, material nonlinear and initial geometric imperfections were considered. The residual stresses caused by roll forming were ignored in finite element analysis because they were reflected in the equivalent constants in Table 2.

#### 3.2.1 Element and material property

When building the finite element model with ABAQUS, the corrugated webs and flanges of W666 ACSR were considered as a thin, laminated composite shell and simulated by S4R5 thin shell elements with an equivalent thickness 1.0 mm. The laminated sections of the webs and bottom flanges in ACSR were defined with the equivalent section properties directly. In Fig. 14, 1-direction is along the longitudinal tangent direction of the arched panel units, 2-direction is parallel to the small corrugations in the webs and bottom flanges, and the 3-direction is normal to the web or bottom flange, then the equivalent orthotropic elastic material properties of the webs and bottom flanges were input as LAMINA type in ABAQUS, in the forms of  $E_1$ ,  $E_2$ ,  $\mu_{12}$ ,  $G_{12}$ ,  $G_{13}$  and  $G_{23}$ , which had been partly obtained from experiments, as shown in Table 2. Because of measurement complication, the shear modulus  $G_{13}$  and  $G_{23}$  were not measured and all assumed to be as same as the upper flange. Considering the relationship in Eq. (2), only  $\mu_{12}$  needed to be input for the two equivalent Poisson's ratios in Table 2.

In order to perform an elastic-plastic analysis in ABAQUS and get the ultimate strength and failure modes, the equivalent  $\sigma$ - $\varepsilon$  curves of the webs and flanges were all assumed to the two-segment lines, and the yield stresses are considered as same as the upper flanges.

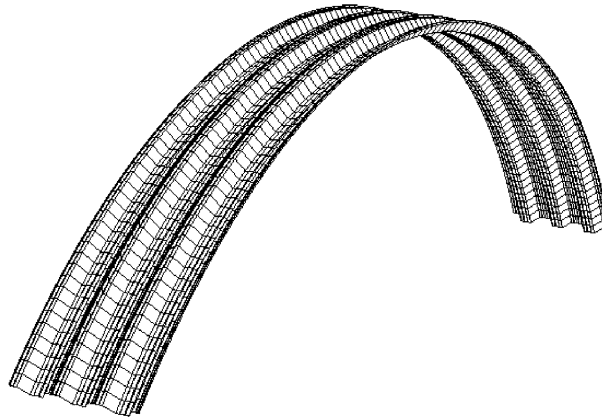


Fig. 15 Mesh of 18 m span W666 ACSR

Because there are no transverse corrugations in it, the upper flange of ACSR also can be simulated by S4R5 thin shell elements with isotropic material properties. Base on the tensile test to the same batch of steel strip, the average thickness of the upper flanges of T18-F and T18-H is 1.06 mm, and the average elastic modulus, yield stress and ultimate stress are separately  $196 \times 10^3 \text{ N/mm}^2$ ,  $310 \text{ N/mm}^2$  and  $365 \text{ N/mm}^2$ . The measurement data are basement of defining the material properties of upper flanges when building the finite element models of 18 m span W666 ACSR samples.

### 3.2.2 Loading, support and mesh

The vertical centralized loads on the ACSR samples in Figs. 8 and 9 were simulated with body forces in the structures when building the finite element models. For the 18 m span W666 ACSR, two loading ways were considered: full and half span loads. According to the actual testing situation, two arch feet were simply taken as the pinned-end support, while the two longitudinal side edges of the analysis model were assumed to the up and down sliding condition. For the sake of reducing the element and joint numbers and saving the analysis time, the mesh sizes of the finite element models were all set as 200 mm. Fig. 15 shows the mesh of the 18 m span W666 ACSR.

### 3.2.3 Introduction of geometric imperfections

In ABAQUS analysis, the Riks method can be used to solve the post buckling problems, which can be accomplished by introducing a geometric imperfection pattern in the “perfect” geometry. ABAQUS offers three ways to define an imperfection. In this paper, the geometric imperfections were defined as a linear superposition of free vibration modes. Because all the failure modes of ACSR samples under full and half span loads are asymmetric base on the testing results, the mode 1, i.e., the asymmetric vibration mode was directly considered as the geometric imperfection shape, in which the maximum values were assumed as  $H/1000$ , i.e. 4.5 mm ( $H$  is the arch rise of 18 m span ACSR).

## 4. Results of testing and finite element analysis

### 4.1 Deformation

After the steel components and angle poles (total weight 0.555 kN for each loading point) were all

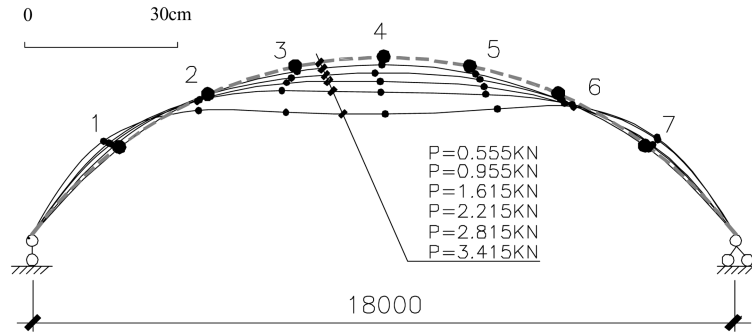


Fig. 16 Deformation shape of sample T18-F under full span loads

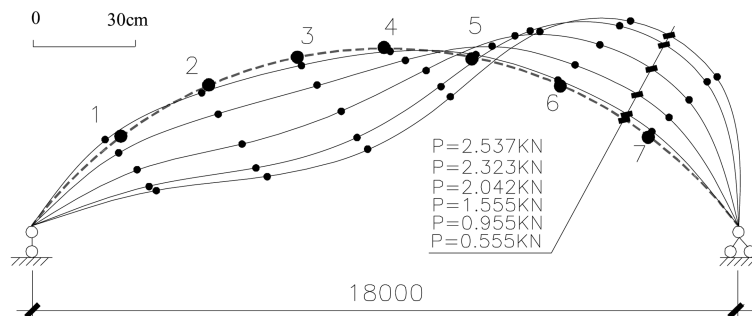


Fig. 17 Deformation shape of sample T18-H under left half span loads

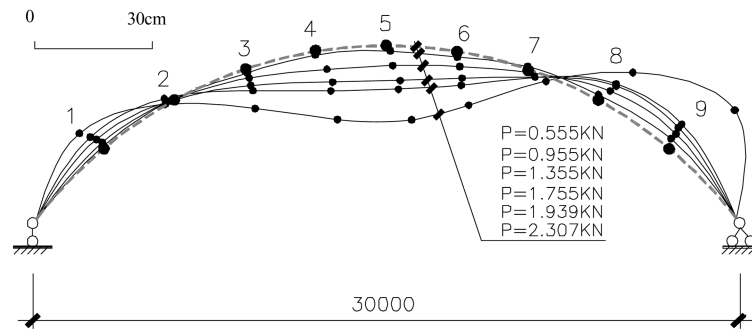


Fig. 18 Deformation shape of sample T30-F under full span loads

fixed on one sample, the structural shape was considered as the initial testing state, i.e., the displacements of the measuring points were assumed to zero. Fig. 16 to Fig. 19 provide the deformation shapes of all four samples under the different testing load levels. Figs. 20 and 21 are the finite element analysis deformation shapes of 18 m span ACSR under no large full and left half spans loads. For the two 18 m span ACSR samples, Fig. 22 shows the relationship between the external load  $q$  ( $\text{kN}/\text{m}^2$ ) and the maximum vertical displacement (Point 4 for full span loading or point 2 for half span loading in Fig. 8) based on the testing and finite element analysis results. For the 30 m span samples, Fig. 23 provides the two load-deflection testing curves, in which the deflections of point 3 or point 5 in Fig. 9

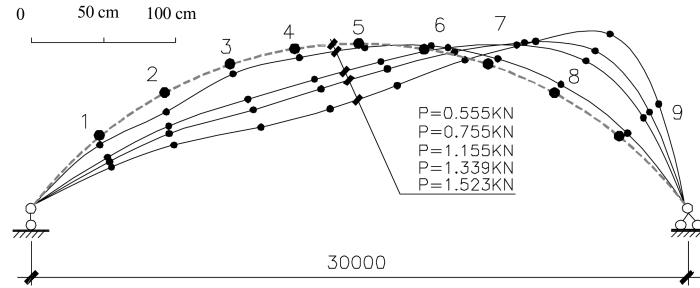


Fig. 19 Deformation shape of sample T30-F under left half span loads

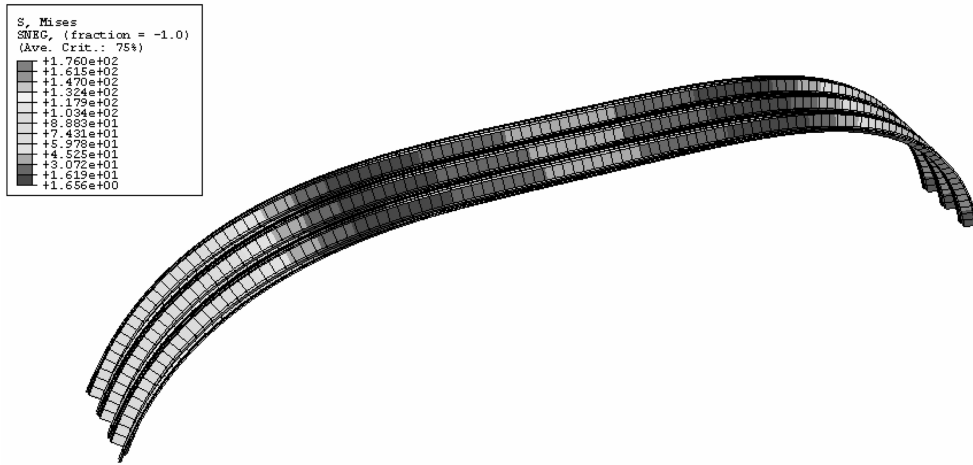


Fig. 20 Symmetric deformation of 18 m span ACSR

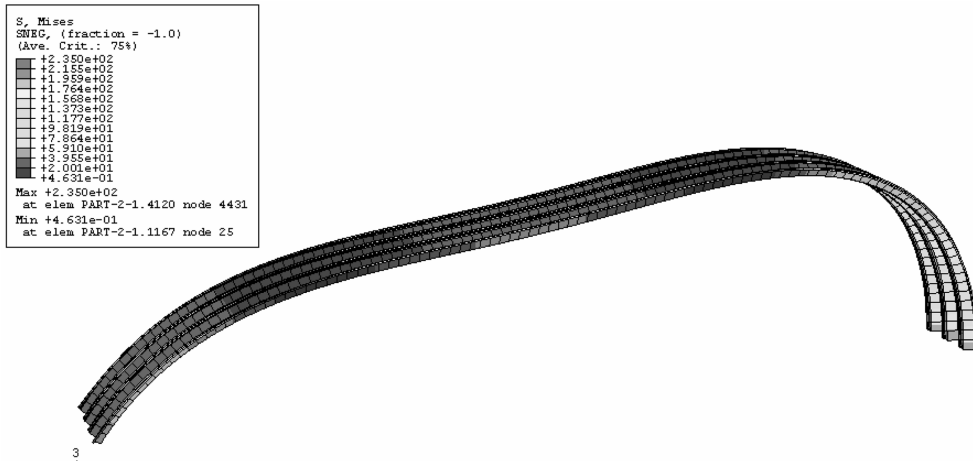


Fig. 21 Asymmetric deformation of 18 m span ACSR

were used for the half or full span loading situations. Base on the above measurement and analysis results, it can be seen that:

1. When the external loads applied along the full span, weather for 18 m or 30 m span samples, the deformation shapes were symmetric, the middle part of the samples went down and the others moved up. But when the external loads approached to the limit values, the failure modes of the samples were asymmetric. For the half span loading situation, the deformation shapes of the samples were asymmetric. As soon as the external loads applied on the arches, the loading sides of the samples began to move down and the other side bulged. The failure modes of the samples are asymmetric.

2. If the displacement under the first level load ( $P = 0.555$  kN) was ignored, when the full span loads got to the maximum values, the measurement vertical displacements at the middle points were 0.111 m ( $L/162, L = 18$  m) for T18-F and 0.188 m ( $L/160, L = 30$  m) for T30-F. For the half span loading, when the loads approached to the maximum values, the measurement vertical and horizontal displacements at the middle points were about 0.144 m ( $L/125, L = 18$  m) and 0.195 m ( $L/92, L = 18$  m) for T18-H; 0.290 m ( $L/103, L = 30$  m) and 0.265 m ( $L/113, L = 30$  m) for T30-H. It is obviously the deformation of ACSR under the vertical loads is large, showing the structural stiffness of ACSR is low. When designing this kind of structure, the allowable deflection should be larger.

3. For the two 18 m span samples under the full and half span loads, the load-deflection curves in Fig. 22 base on the finite element analysis have a good agreement with the testing results, showing the simplify method of small corrugations in ACSR and the building techniques of the finite element analysis models are rational and effective.

#### 4.2 Bearing capacities and failure modes

For each loading point, from began to the last loading level before failure, the total weight, including iron bricks, two hooks, iron wires, three steel components and one angle pole, is considered as the limit bearing capacity  $P_T$  (kN) of the testing sample. Because  $P_T$  is the centralized load, it is transferred to the uniform distributed load  $q_u$  (kN/m<sup>2</sup>) in the horizontal plane. For the finite element analysis, the bearing capacity was determined base on the highest point in the load-deflection curve, as shown in Fig. 22.

According to the testing phenomenon, when the external loads got near to the limit value of a sample, the bottom flange at sample's bulge place locally buckled first, as shown in Fig. 24. This is because that the transverse corrugations in the bottom flanges are deep, the compressive stiffness of the bottom flanges along the arch is low. Several loading levels later, the full sample crinkle buckled at this place

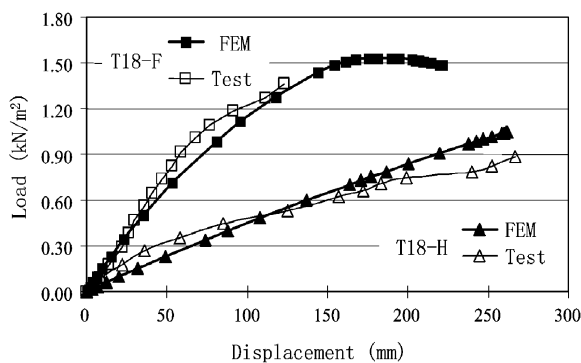


Fig. 22 Relationship between load and vertical displacement of 18 m span ACSR

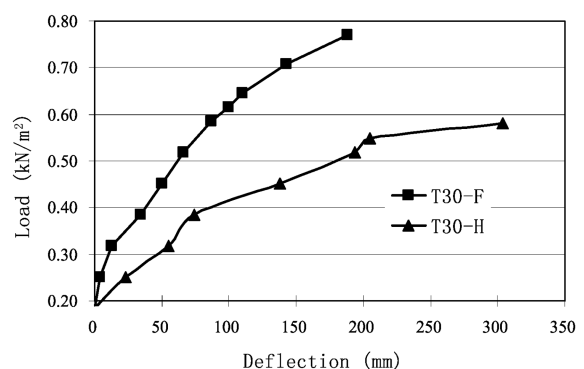


Fig. 23 Relationship between load and vertical displacement of 30 m span ACSR



Fig. 24 Local buckle of bottom flange of 18 m span sample



Fig. 25 Wrinkle buckle of sample T30-F

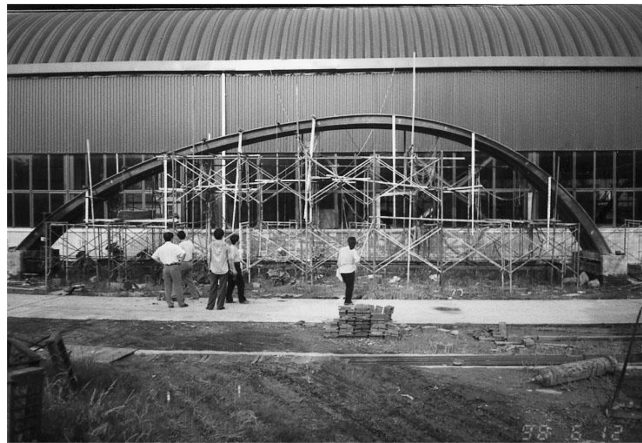


Fig. 26 Failure mode of sample T18-H under left half span loading

Table 3 Limit loads and local buckling places of four samples

Samples	Spans (m)	Loading methods	Testing data		Analysis results		Places of local buckling flanges base on testing
			$P_T$ (kN)	$q_T$ (kN/m <sup>2</sup> )	$q_A$ (kN/m <sup>2</sup> )	$q_T/q_A$	
T18-H	18	Half span	2.537	1.128	1.047	1.077	Left of point 7
T18-F	18	Half span	3.415	1.518	1.531	0.992	Right of point 7
T30-H	30	Half span	1.739	0.580			Point 8
T30-F	30	Full span	2.307	0.769			Left of point 9

Remarks: For half loading, the loadings were applied on the left side

(Fig. 25) and collapsed suddenly (Fig. 26). In the finite element analysis results, the local buckling of T18-F and T18-H did not appear, which is partly because the mesh size 200 mm is large.

Table 3 summarizes the limit bearing capacities and local buckling places of all four testing samples. Base on the table, the limit bearing capacities  $q_T$  of two 18 m span samples are separately 1.128 kN/m<sup>2</sup> and 1.518 kN/m<sup>2</sup> for left half and full span loading situations, and the ration between the two values is

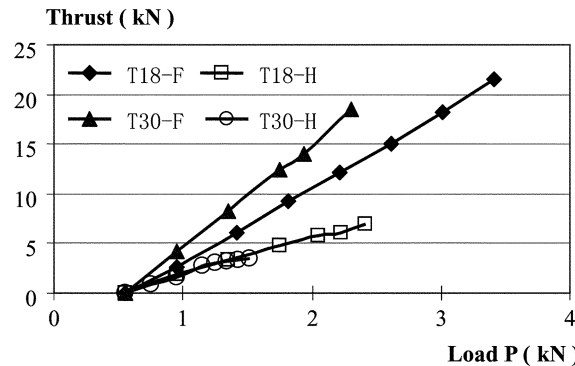


Fig. 27 Relationship between horizontal thrust and load  $P$

74 %. The local buckling places of the bottom flanges are usually 1/8 span away from the right ends. For the sake of comparing, the finite element analysis capacities  $q_A$  of T18-H and T18-F are also provided in Table 3, which are separately 1.047 kN/m<sup>2</sup> and 1.531 kN/m<sup>2</sup>. The bearing capacity ratios  $q_T/q_A$  are 1.077 for T18-H and 0.992 for T18-F, showing the simplify method of small corrugations in ACSR and the building techniques of finite element models are rational and accurate.

For the two 30 m span samples, the limit loads are separately 0.580 kN/m<sup>2</sup> and 0.769 kN/m<sup>2</sup> for T30-H and T30-F, and the ratio between the two values is 75 %. The local buckling place of the bottom flange is 1/10 span away from the right end for full span loading, while 1/5 span away for the left half loading.

The test and analysis results prove that the loading capacities of W666 ACSR are low, and the half span vertical loading situation is more dangerous. This kind of thin walled structure can be used in the structures under small external vertical loads.

### 4.3 Horizontal thrust

The horizontal thrust was obtained from the sum values of the three 50 kN load cells, set in the middle of the three steel bars. Fig. 27 shows the relationship between horizontal thrust and external load  $P$  for all four samples. It is obvious that there is a linear relationship between the two parameters. For the same span and external load  $P$ , the horizontal thrust of the full span loading is about 2 times as half span loading.

## 5. Conclusions

In this paper, a kind of W666 Arched Corrugated Steel Roof (ACSR) is considered as the research object. Four full-scale samples, including two 18 m and two 30 m span ones, were tested under the external static vertical loads. The web and bottom flange are separately simplified to anisotropic uniform curved plates and the equivalent average tensile modulus, shear modulus and Poisson's ratio were measured by tensile and shear tests. The two 18 m-span W666 ACSR were analyzed with the finite element analysis program ABAQUS. The deformation, limit bearing capacities and failure modes of the samples were measured and analyzed. Base on the testing and analysis results, the limit vertical bearing capacity of W666 ACSR is low, and this kind of structure can be used in the situation with small vertical loads. For half span loading, the limit bearing capacity is 74-75% compared with the full

span loading base on tests. The bottom flange locally buckles at the sample's bulge place first, then the full structure wrinkle buckles and collapses. When the external load applies along the full span of the structure, the deformation shape is symmetric, but the failure mode of the sample is asymmetric. For the situation of half span loading, the deformation shape and the failure mode of the structure are all asymmetric. The measurement and theory analysis results show that the vertical displacement of ACSR under the vertical loads is large and the stiffness of ACSR is low. There is a linear relationship between the external load and the horizontal thrust. There is a small difference between the finite element analysis results and testing data, showing the simplify method of small corrugations in ACSR and the building techniques of the finite element analysis models are rational and useful.

## Acknowledgements

This paper is supported and funded by Hubei Province Construction Department (K200502) and Wuhan Iron and Steel (Group) Company. The authors are also grateful to the technicians in Structural Laboratory, School of Civil Engineering and Architecture, Wuhan University of Technology.

## Reference

- Abdel-Sayed, G. (1970), "Critical shear loading of curved panels of corrugated sheets", *J. Eng. Mech. Div.*, **96**(6), 895-912.
- Airumyan, E. L. and Boyko, O. I. (1997), "Full-scale testing and design of frameless arch steel roof", *Struct. Assessment*, BookWeb Pro, London, 211-218.
- Benussi, F. and Mauro, A. (1986), "Half-Barrel shells composed of cold-formed profiles", *Proceedings of IABSE Colloquium*, Stockholm, June.
- CECS167 (2004), "Technical specification for arched corrugated steel roof", *China Association for Engineering Construction Standardization* (In Chinese), China Planning Press, Beijing.
- Featherston, C. A. and Ruiz, C. (1998), "Buckling of curved panels under combined shear and bending", *J. Mech. Eng. Sci. Proceedings Part C*, **212**, 183-196.
- Friedman, R. and Kennedy, J. (1994), "Analysis and compression testing of 2024 and 8009 aluminum alloy zee-stiffened panels", *J. Eng. Mater. Technol.*, Trans AMSE, **116**(2), 238-23.
- Hahn, E. K., Carlsson, L. A. and Westerlind, B. S. (1992), "Edge-compression fixture for buckling studies of corrugated board panels", *Exp. Mech.*, 252-258.
- Herbert, A. M. and Smith, J. H. (1976), "Finite element analysis of doubly corrugated shells", *J. Struct. Div.*, **102**(10), 2033-2051.
- Jorgenson, J. L. and Chowdhury, A. H. (1982). "Buckling strength of cold-formed steel curved panels", *Proceedings of Sixth International Speciality Conference in Cold-formed Steel Structures*, ST. Louis, Missouri, Nov.
- Liu, Xiliang, Zhang, Yong and Zhang, Fuhai (1999), "Experimental study on full-sized models of arched corrugated metal roof", *Proceedings of ICASS'99*, Hong Kong, December.
- Marzouk, O. A. and Abdel-Sayed, G. (1975), "Stability of half-barrel orthotropic shells", *J. Struct. Div.*, **101**(7), 1517-1530.
- Wang, Xiaoping (1999), "Experimental study and FEM analysis of large-span metal corrugated arch roof", PHD thesis (In Chinese), Wuhan University of Technology.
- Xu, Lei, Gong, Yanglin, Guo Ping (2001), "Compressive tests of cold-formed steel curve panels", *J. Construct. Steel Res.*, **57**, 1249-1265.
- Zhang, Yong (2000), "Study on analysis theory, design method and experiments of arched corrugated metal roof", PHD thesis (In Chinese), Tianjin University.